High-Pressure NMR Reveals Volume and Compressibility Differences Between Two Stably Folded Protein Conformations

Xingjian Xu[1,2], Donald Gagné[1, †], James M. Aramini[1], Kevin H. Gardner[1,3,4,]*

[1]Structural Biology Initiative, CUNY Advanced Science Research Center, New York, NY

[2]Ph.D Program in Biochemistry, The Graduate Center, CUNY, New York, NY

[3]Department of Chemistry and Biochemistry, City College of New York, New York, NY

[4]Ph.D. Programs in Biochemistry, Chemistry and Biology, The Graduate Center, CUNY, New York, NY

†: current address: Kisoji Biotechnology, Montréal, QC, Canada

[*]: address correspondence to:

Kevin Gardner, Structural Biology Initiative, CUNY Advanced Science Research Center, 85 St. Nicholas Terrace, New York, NY 10031 USA, E-mail: kgardner@gc.cuny.edu; phone: +1 212 413 3220

Authors ORCIDs:

Xingjian Xu: 0000-0002-9609-4755

Donald Gagné: 0000-0002-3938-6567

James M. Aramini: 0000-0001-8926-4210

Kevin H. Gardner: 0000-0002-8671-2556

ABSTRACT

Proteins often interconvert between different conformations in ways critical to their function. However, manipulating the equilibrium positions and kinetics of such conformational transitions has been traditionally challenging. Pressure is an effective thermodynamic variable for favoring the population of high energy protein conformational states with smaller volumes, as elegantly demonstrated in its use for biophysical studies of unfolding transitions. Here, we investigate the pressure-dependent effects of the interconversion of two stably-folded conformations of the Y456T variant of the aryl hydrocarbon receptor nuclear translocator (ARNT) Period/ARNT/Single-minded PAS-B domain. We previously discovered that ARNT PAS-B Y456T spontaneously interconverts between two structures primarily differing by a three-residue β-strand slip, inverting its topology in the process. This change collapses the internal cavities of the WT-like (WT) conformation of this protein as it adopts the slipped conformation (SLIP). Using pressure-NMR to conduct thermodynamic and kinetic analyses of the interconversion of ARNT PAS-B, we provide data that support two key predictions of this process: the SLIP conformation is both smaller and less compressible than the WT conformation, and the interconversion proceeds through a chiefly-unfolded intermediate state. We also find that the pressure-dependent NMR chemical shift changes and the residue-specific compressibility both predict which amino acid residues are near protein cavities. We demonstrate that pressure-NMR is a powerful approach for characterizing protein conformational switching and can provide unique information that is not easily accessible through other techniques.

Keywords. ARNT; Per-ARNT-Sim domains; high pressure NMR; cavities; conformational change; compressibilities

INTRODUCTION

The energy landscape theory of protein folding states that a protein samples many conformations along its folding energetic landscape before reaching the native state [1-2]. Although the native conformation of a protein is usually the lowest free energy state under physiological conditions, proteins can in fact be trapped in non-native, stably-folded local minima with substantially different structures than the native conformation [3-5]. Transitions between these states, which can be spontaneous or triggered by changes in pH, temperature, or ligand binding, are often critical for shifting proteins between functionally inactive and active forms [3-7]. Taken to an extreme, one arrives at the emerging concept of 'metamorphic' proteins, where one sequence can reversibly adopt different stable folds in different environmental conditions [8-10]. However, identifying and characterizing high energy states of a protein can be challenging, as these are sparsely populated by definition [11-12]. Several techniques are currently available for quantitative characterization of conformational sub-states, predominately through modeling, molecular dynamics simulations, and advanced nuclear magnetic resonance (NMR) techniques such as relaxation dispersion experiments [11-14]. One can also access these excited states by stabilizing them using small molecule ligands and chemical denaturants or by changing experimental conditions, e.g. changing pH or temperature [11, 15-17]. A less-commonly used environmental variable, pressure, has gained interest as pressure-manipulating equipment compatible with standard biophysics instrumentation become more readily accessible [18-20]. Pressure directly affects protein conformational equilibria by acting on differences in the partial volumes and compressibilities of different conformers, with increasing pressure favoring conformations with lower volumes [21]. As such, pressure tends to denature proteins as unfolded proteins are generally smaller than their folded forms; such transitions typically occur above 2000 bar under native

69 conditions [20-25]. However, the application of sub-unfolding pressures can often cause proteins to
70 shift populations among multiple folded states [18, 26-28], providing an easily applied (and removed)
71 way to manipulate protein conformational equilibria to facilitate their study.

72 These advantages of pressure-NMR led us to examine their applicability to a domain
73 from the ARNT (Aryl hydrocarbon Receptor Nuclear Translocator) protein which we knew to be
74 in slow conformational exchange between two folded states [29-30]. ARNT is a bHLH-PAS (basic
75 helix-loop-helix / Per-ARNT-Sim) protein that heterodimerizes with other bHLH-PAS proteins
76 to form transcription factor complexes in response to a variety of environmental stimuli [31]. Many
77 of the interactions between ARNT and its binding partners are mediated by two tandem PAS
78 domains, PAS-A and PAS-B. Each PAS domain has an antiparallel five-stranded β-sheet packed
79 against several α-helices (Cα, Dα, Eα, Fα) on one side, often encapsulating internal cavities
80 between them [31-33]. The β-sheet surface of the PAS domain is an important binding interface for
81 intermolecular interactions [31, 33]; for ARNT PAS-B, it is essential for a diverse array of
82 interaction partners, including other PAS domains, as well as co-activators and cofactors [31-35].
83 The protein-protein interactions at the β-sheet surface are central to the variety of roles ARNT
84 plays in signaling pathways [29, 32, 36-37]. Notably, the ability of small molecules to bind within
85 internal cavities also provides the possibility to control these pathways with artificially designed
86 ligands [32].

87 While previously characterizing ARNT PAS-B point mutants, we surprisingly discovered
88 that its β-sheet is highly sensitive to a single residue preceding the final strand (Iβ) at residue 456
89 [29]. A single change at this site (Y456T) creates a stably-folded alternative conformation in a 1:1
90 equilibrium with the WT conformation, with the two conformers slowly and reversibly
91 interconverting with each other [29-30] (**Fig. 1**). Additional mutations to nearby residues

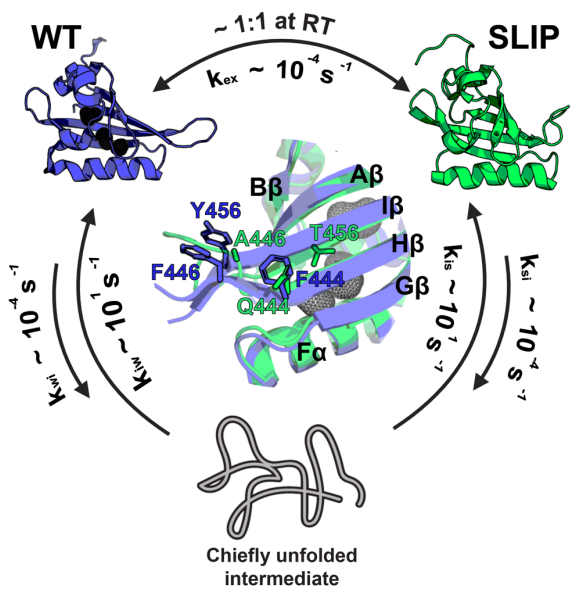

Figure 1. Current model of ARNT PAS-B Y456T interconversion between the WT and SLIP conformation. Prior studies have shown this protein interconverts between the folded WT and SLIP conformations on the same timescale as the unfolding rates of either conformer, implying a slow transition process requiring a chiefly unfolded intermediate state. The two conformations are in 1:1 equilibrium at room temperature, but favors the SLIP conformation at lower temperature, in 1:1.5 equilibrium at 278.1K. The F444Q/F446A/Y456T variant (TRIP) locks the protein in the SLIP conformation, structural comparison between WT and TRIP (WT slate blue, SLIP lime green) is displayed in the middle, with mutation sites labeled.

(F444Q/F446A/Y456T, hereafter called the TRIP variant) stabilize the alternative conformation to a 99:1 abundance over the WT conformation, letting us characterize the alternative conformation. While the bulk of the new conformation retains the same structure as WT, the Iβ-strand 'slips' by three residues in the new SLIP conformation. This slip is accompanied by a corresponding topology inversion, abolishing the domain's ability to interact with some other binding partners [29]. We believe that the bulky tyrosine side chain at position 456 prevents a similar slip of the Iβ-strand in the WT protein, while the smaller threonine side chain of Y456T can move from a solvent-exposed position into an internal cavity [29-30]. Since the Iβ-strand inversion flips additional solvent-exposed side chains into the cavities in the SLIP conformation, these internal cavities shrink in size as established by our in-house cavity-searching algorithm [15].

102 The volume difference between the two states makes this system ideal for pressure perturbation
103 studies, with the application of pressure predicted to favor the smaller SLIP state [18, 38-41].

104 To explore the pressure dependence of thermodynamic and kinetic parameters of the
105 WT:SLIP interconversion, we used high-pressure solution NMR approaches to study ARNT
106 PAS-B Y456T at pressures between 20 and 2500 bar. Data from these studies let us establish the
107 pressure dependencies of both the conformational equilibrium and the interconversion rate.
108 Interestingly, we found that the WT conformation is larger in both its internal volume and
109 compressibility than the SLIP conformation. We attributed these differences to the internal
110 cavities uniquely found in the WT conformation [29, 32]. Additionally, we tested a hypothesis that
111 WT:SLIP interconversion proceeds through a chiefly unfolded intermediate state, previously
112 established on a kinetic argument that the unfolding and interconversion rates are similar. We
113 found data supporting this hypothesis via measurements of the internal volume and
114 compressibility of that transition state [30], further bolstered by pressure-dependent unfolding
115 profiles of the ARNT PAS-B WT and TRIP mutant that locks the protein in one of the two
116 conformations. Finally, we report that both residue-specific compressibility and pressure-
117 dependent chemical shift changes can predict whether residues are near cavities. These data also
118 establish that residues associated with cavities and ligand binding in WT are rigidified in TRIP,
119 as indicated by the differences in nonlinear chemical shift coefficients between the two states.
120 Using ARNT PAS-B as a test case, we show high-pressure NMR as a robust tool to apply
121 reversible perturbation of protein populations, enabling both thermodynamic and kinetic
122 analyses. Such approach can be easily adopted to studies of other protein equilibrium transitions
123 by stabilizing conformations and/or perturbing transition states.

124 **MATERIALS AND METHODS**

125 **Protein Purification and Expression**

126 His_6-tagged human ARNT PAS-B (residues 356-470) WT and mutants (Y456T and
127 F444Q/F446A/Y456T) were uniformly labeled with ^{13}C and ^{15}N and overexpressed in BL21
128 (DE3) E. coli. Isotopically-labeled proteins were obtained by growing cells in M9 media
129 supplemented with 3 g/L U-$^{13}C_6$ glucose and 1 g/L $^{15}NH_4Cl$ as the carbon and nitrogen sources,
130 respectively. Cells were incubated at 37 °C until an OD_{600} of 0.6-0.8. Protein expression was
131 induced with 0.5 mM Isopropyl-β-D-thiogalactopyranoside (IPTG) and incubated overnight (~
132 16-18 hr) at 18 °C. Cells were harvested next day, cell pellets were resuspended in 50 mM Tris
133 (pH 7.5), 150 mM NaCl, 10 mM imidazole, 1 mM DTT buffer containing 1 mM PMSF, lysed
134 with sonication, and centrifuged. Supernatant was incubated with 5 mL of Ni^{2+} Sepharose™
135 High Performance beads and eluted with 500 mM imidazole buffer. His_6-Tagged ARNT PAS-B
136 proteins were exchanged into a low imidazole buffer (8 mM imidazole, 50 mM Tris (pH 7.5),
137 150 mM NaCl, and 1 mM DTT) and incubated overnight with His_6-tobacco etch virus (TEV)
138 protease for tag cleavage. The freed His_6-tag and His_6-TEV were removed by a second round of
139 Ni^{2+} column purification. ARNT PAS-B proteins were further purified by passing through a
140 Superdex 75 size exclusion column and exchanged into baroresistant buffer (44.7 mM Tris pH
141 7.0, 5.3 mM phosphate, 17 mM NaCl, 1 mM DTT) [42] and concentrated with an Amicon stirred
142 ultrafiltration unit with a 3 kDa filter to 320 μM. Samples were flash frozen with liquid nitrogen
143 and were stored at -80 °C for later use.

144 **Pressure-Jump NMR Experiments**

145 Solution NMR experiments were performed on a Bruker Avance III HD 700 MHz NMR
146 spectrometer equipped with a 5-mm QCI-F cryoprobe. NMR samples were prepared by mixing

147 80% of the purified protein samples with 20% D_2O yielding a final concentration of around 250
148 μM. Samples were loaded into a commercially-available pressure resistant NMR cell (Daedalus
149 Innovations, Aston, PA, USA), with pressure between 20 bar to 2500 bar applied through a
150 Xtreme-60 Syringe Pump from the same vendor. The baseline pressure was set to 20 bar as it is a
151 low pressure that can be stably maintained by the pump. We performed two types of pressure-
152 jump experiments, direct pressure-jump experiments where pressure was increased directly from
153 20 bar to the destination pressure of up to 2500 bar, and cumulative step pressure-jump
154 experiments with constant intervals, where pressure was increased incrementally from baseline
155 pressure to the final pressure of 2500 bar. To set up direct pressure-jump experiments, samples
156 were thawed and stored on ice, and first equilibrated at 20 bar and 278.1 K for 1 hr and raised to
157 a higher pressure (between 125 bar to 1500 bar) and equilibrated at that pressure. As identified in
158 preliminary experiments, the duration of equilibration process varies depending on the pressure:
159 interconversion of the two populations at 20 bar takes around 12 hours to complete, while it
160 occurs more quickly as pressure increases [30]. Equilibration time under pressure was therefore set
161 to 12 hr at 125 bar, and gradually reduced to 5 hr for pressures between 500 to 1000 bar, and
162 finally 4 hr for pressures beyond 1000 bar. During the equilibration, a series of 1D ^{13}C edited ^{1}H
163 NMR experiments were recorded to detect the rate of interconversion, with each spectrum
164 requiring ca. 4.25 min to acquire. The system was relaxed for 12.5 hr at 20 bar post
165 equilibrations at different pressures, 1D ^{13}C-edited ^{1}H NMR experiments were also recorded
166 during relaxation. For step pressure-jump experiments, samples were first equilibrated at 20 bar
167 and 278.1K, then pressurized and equilibrated in steps of 250 bar, until reaching 2500 bar.
168 Equilibration time was set to 9 hr at 250 bar, 6 hr at 500 bar, 5 hr for 750 and 1000 bar, and 4 hr
169 for 1250, 1500, 1750, 2000, and 2250 bar. Equilibration time was extended to 6 hr at 2500 bar to

170 monitor any unfolding effects at the highest pressure safely accessible with our instrumentation.
171 1D NMR spectra were acquired as described earlier. $^{15}N/^{1}H$ and $^{13}C/^{1}H$ HSQC spectra were also
172 acquired at system equilibrium at 20, 250, 500, 750, 1000, 1250, 1500, and 2500 bar. $^{15}N/^{1}H$
173 HSQC experiments were acquired with 16 scans and FIDs of 2048x256 complex points. $^{13}C/^{1}H$
174 HSQC experiments were acquired with 8 scans and FID of 2048x256 complex points. All NMR
175 spectra were processed and analyzed with NMRFx Analyst and NMRViewJ [43-44]. Chemical shift
176 assignments from previous NMR assignments of ARNT PAS-B WT and F444Q/F446A/Y456T
177 mutant were used for all analyses [29-30].

178 Unfolding measurements of ARNT PAS-B WT and the F444Q/F446A/Y456T variant
179 under pressures accessible by our apparatus (20-2500 bar) was achieved by the addition of urea
180 (up to 3.0 M). $^{15}N/^{1}H$ HSQC spectra were acquired between 20 and 2500 bar with increments of
181 250 bar. Peak assignments from previous work were obtained [29, 31], and transferred to the
182 acquired spectra following urea titration experiments between 0.5 and 3.0 M.

183 **NMR Data Analysis**

184 In the 1D ^{13}C-edited ^{1}H NMR experiments, two peaks corresponding to the L391-δ1
185 methyl group of the WT and SLIP conformations were used to determine the populations of each
186 conformational state of the protein in the sample. The relative populations (SLIP/WT) at
187 different pressures were obtained by taking the ratio of the integrals of the two peaks. The
188 equilibration (change in relative population) under different pressures and the rates of
189 interconversion were obtained by plotting the relative population as a function of time.

190 The equilibrium constant K between the two conformers of the ARNT PAS-B Y456T is
191 given by the relation

$$K = \frac{[SLIP]}{[WT]} = e^{-\Delta G/RT} \qquad (1)$$

Since the temperature T was kept constant during the pressure jump experiments, the free energy ΔG scales only with pressure p. The free energy as a function of pressure can be approximated by a Taylor expansion

$$\Delta G(p) = \Delta G^0 + \Delta V^0 (p - p_0) - \frac{1}{2} \times \Delta\beta V^0 (p - p_0)^2 + \ldots \frac{\Delta G^n (p_0)}{n!} (p - p_0)^n \qquad (2)$$

ΔG^0 is the free energy between the two conformers at ambient pressure, ΔV^0 is the volume difference between the two conformers, representing the first derivative of free energy with respect to pressure, and compressibility between the two conformations, $\Delta\beta V^0$, is the second derivative of free energy, with respect to pressure. The equilibrium constants were plotted as a function of pressure, and fit to the following equation, incorporating up to the third term of the Taylor series [18]:

$$K_{eq} = e^{-\left(\Delta G^0 + (p - p_0)\Delta V^0 - 1/2 \times \Delta\beta V^0 (p - p_0)^2\right)/RT} \qquad (3)$$

The pressure was referenced to atmospheric pressure, p_0=1 bar.

The observed rate of increase of one conformation (or decrease of the other conformation) as a function of pressure could be fit to a biexponential equation:

$$k_{obs} = k_{sw0} e^{-\left(p\Delta V_{sw}^{\ddagger} - 1/2\Delta\beta V_{sw}^{\ddagger} p^2\right)/RT} + k_{ws0} e^{-\left(p\Delta V_{ws}^{\ddagger} - 1/2\Delta\beta V_{ws}^{\ddagger} p^2\right)/RT} \qquad (4)$$

yielding the activation volumes ($\Delta V_{sw}^{\ddagger}$ and $\Delta V_{ws}^{\ddagger}$) and compressibility differences between the two folded conformations (WT and SLIP) to the previously-proposed, chiefly unfolded intermediate state ($\Delta\beta V_{sw}^{\ddagger}$ and $\Delta\beta V_{ws}^{\ddagger}$) [30]. Together with the two initial rate constants at ambient pressure

(k_{sw0}, SLIP to WT, and k_{ws0}, WT to SLIP), there were 6 unknown parameters to be fit. To better approximate the two exponential terms, rates at different pressures were solved numerically using the following differential equation pair:

$$\frac{d[S]}{dt} = -k_{sw}[S] + k_{ws}[W] \qquad (5)$$

$$\frac{d[S]}{dt} = k_{sw}[S] - k_{ws}[W] \qquad (6)$$

The fittings were done in R, using the package deSolve as the ordinary differential equation solver, and Levenberg-Marquardt Nonlinear Least-Squares Algorithm in minpack.lm for parameter fitting [45].The uncertainty of the fitting was estimated by calculating the 95% confidence intervals from the variance covariance matrix of the fit rate constants. 95% confidence intervals were further verified with a bootstrapping procedure. Random noises with mean of 0 and variance of the mean square error from the model were added to the raw data and fit repeatedly. The estimated parameters were computed to determine if they fall within the 95% confidence interval. k_{sw} and k_{ws} obtained were plotted separately as functions of pressure, and fit individually to:

$$k_{sw} = k_{sw0} e^{-\left(p\Delta V_{sw}^{\ddagger} - 1/2\Delta\beta V_{sw}^{\ddagger} p^2\right)/RT} \qquad (7)$$

$$k_{ws} = k_{ws0} e^{-\left(p\Delta V_{ws}^{\ddagger} - 1/2\Delta\beta V_{ws}^{\ddagger} p^2\right)/RT} \qquad (8)$$

obtaining rates at ambient pressure, activation volumes, and activation compressibilities as described earlier.

229 The temperature dependence of the relaxation rates was calculated as the apparent rates
230 during the 1000 to 20 bar re-equilibration step at temperatures of T = 278.1, 283.1, 288.1, and
231 291.1 K. The change of relative population ([SLIP]/[WT]) over time was fit to a single
232 exponential with the apparent rate of

233 $$k_{app} = k_{ws} + k_{sw} \qquad (9)$$

234 An Eyring relationship between rate and temperature was found by plotting ln(k_{app}/T) against
235 1/T. The plot was fit to a linear equation to extract the entropic and enthalpic contributions of
236 activation energy of transition from SLIP to WT during relaxation at 20 bar.

237 For the pressure-dependent unfolding experiments, ^{15}N/^{1}H HSQC spectra at different
238 pressures were collected, maximum peak intensities in each spectrum were obtained and
239 compared with the peaks corresponding to the same residues collected at different pressures.
240 Overlapping peaks were excluded from the analysis. The intensity averages at different pressures
241 were plotted as a function of pressure, and fit to a two-state unfolding model with XMGrace [46],

242 $$\frac{I}{I_0} = \frac{e^{-\left(\Delta G_f^0 + P\Delta V_f\right)/RT}}{1 + e^{-\left(\Delta G_f^0 + P\Delta V_f\right)/RT}} \qquad (10)$$

243 where I_0 is the peak intensity at initial (20 bar) pressure, R is gas constant, and T is temperature.
244 The apparent volume difference between the folded and unfolded state (ΔG_f^0) and the free energy
245 of folding (ΔV_f) were extracted. For simplicity, the max and min plateau values were set to 1 and
246 0.

247 For the pressure-jump ^{15}N/^{1}H HSQC experiments, we analyzed the peaks under different
248 pressures and determined the change in chemical shifts and intensity under pressures compared

249 to the reference chemical shift (positions of peaks at 20 bar). We fit the change in chemical shifts
250 to the following equation to determine the nonlinear coefficients[18, 26, 47]:

251 $$\Delta\delta_i = b_i \Delta p + c_i \Delta p^2 \qquad (11)$$

252 Where p is pressure (bars), b_i (parts per million per bar) and c_i (parts per million per square bars)
253 are the first and second order pressure dependence coefficients on chemical shifts for the ith
254 residue. A large c_i value suggests high nonlinear response to pressure. Fittings were performed
255 with the built-in pressure-analysis function of NMRViewJ [43]. Residue-specific nonlinear
256 coefficient differences between the two conformations were calculated by subtracting the
257 absolute values of c_i corresponding to each conformation:

258 $$\Delta c_i = |c_{iwt}| - |c_{islip}| \qquad (12)$$

259 Values were mapped to the crystal structure of WT ARNT PAS-B [48] and visualized with PyMOL
260 (The PyMOL Molecular Graphics System, Version 2.0 Schrödinger, LLC).

261 **Void Volume Calculation**

262 Void volumes of ARNT PAS-B WT and SLIP conformations were calculated with the
263 ProteinVolume software package by Chen and Makhatadze [49]. Briefly, the total solvent-excluded
264 volume of the protein is calculated by filling the space within the protein's molecular surface
265 with 0.02 Å probes. The van der Waals volume is calculated with the same process but only
266 counting the probes that are within the van der Waals radius of any atoms. The void volume V_{void}
267 is given by the difference between the two volumes calculated. Solution NMR structures of WT
268 and SLIP were used for the calculation [29, 31], using the average void volume of all 20 conformers
269 in these ensembles.

RESULTS

Equilibrium Analyses: Pressure Dependence of ARNT PAS-B Conformation Equilibrium

We previously determined the solution and crystal structures of WT ARNT PAS-B and the solution structure of ARNT PAS-B F444Q/F446A/Y456T (TRIP) variant [29, 31-32]. The crystal structures of larger ARNT bHLH-PAS fragments bound to a number of bHLH binding partners have also been elucidated [33, 35]. Here we compared the average void volumes of the two solution structure ensembles with ProteinVolume [49], and found that the SLIP conformation had approximately 600 $Å^3$ smaller void volume than WT, leading us to hypothesize that the equilibrium between these conformations would be pressure sensitive. To test this hypothesis, we used pressure jump NMR by applying cumulative 250 bar pressure jumps (20, 250, 500, … up to 2500 bar) to ARNT PAS-B Y456T and acquiring $^{15}N/^{1}H$ and $^{13}C/^{1}H$ HSQC spectra at each pressure once the system equilibrated to each change. By overlaying these spectra (**Fig. 2A, S1)**, we noticed all three (^{1}H, ^{15}N, ^{13}C) nuclei showed pressure-dependent changes in chemical shifts and relative population between the two conformations, as predicted from the volume differences between them. In general, we observed that increased pressure decreased the intensities of WT signals while concomitantly increasing SLIP signal intensities, confirming the smaller calculated volume of the SLIP conformation [30].

To explore the reversibility of pressure-induced WT:SLIP conformational shifts within the pressure range of our study, we recorded spectra of ARNT PAS-B Y456T at 20 bar both before and after raising the sample pressure to 2500 bar. Comparison of the 20 bar spectra recorded before and after this jump showed no significant differences (**Fig. S2**), suggesting reversibility for short periods of time at pressures up to at least 2500 bar.

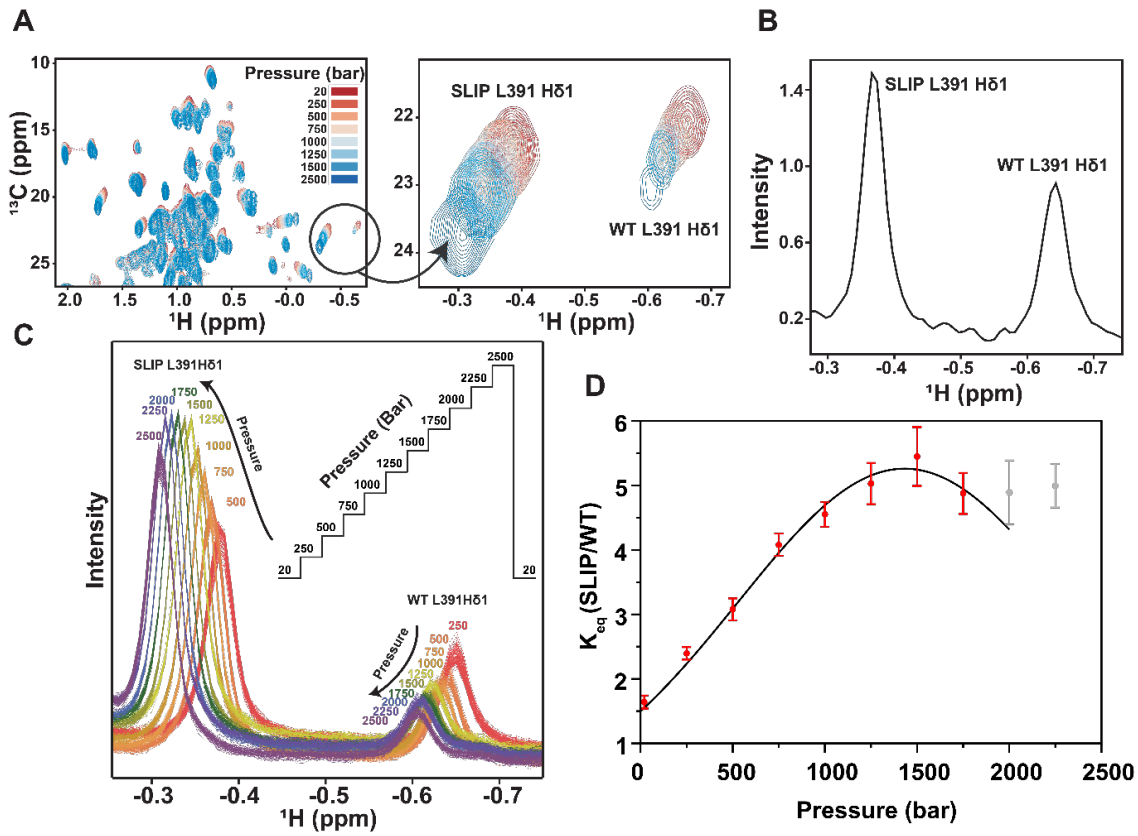

Figure 2. Pressure-induced equilibrium shift between WT and SLIP conformation of ARNT PAS-B Y456T. A) Methyl region of ^{13}C/^{1}H HSQC spectra of ARNT PAS-B Y456T recorded after equilibration at multiple pressures between 20-2500 bar. Equilibrium shift at different pressures is visualized by comparing the conformer-dependent peaks of several sites, including the L391 δ1 methyl group. B) ^{13}C-edited 1D ^{1}H NMR of L391 Hδ1 equilibrated at 278.1K and 20 bar. K_{eq} (SLIP: WT) is approximately 1.5, as assessed by the areas of the two conformer-specific peaks. C) ^{13}C-edited 1D ^{1}H NMR of L391 Hδ1 recorded at pressures between 20-2500 bar as shown in inset. Spectra were collected during sample equilibration at each pressure. D) Fitting pressure dependence of equilibrated K_{eq} from datasets shown in C. K_{eq} above 1750 bar are not included for the fitting as another SLIP peak moves close to SLIP L391 δ1, interfering with the baseline and leading to overestimation of the SLIP population.

To thermodynamically and kinetically characterize the interconversion between the WT and SLIP conformations, we acquired a series of ^{13}C-edited 1D ^{1}H NMR spectra during the equilibration periods as pressure changed. We have previously shown that the L391 Hδ1 methyl signal of both WT and SLIP conformations are particularly upfield shifted and well resolved in multiple types of NMR spectra, likely due to its location adjacent to a cavity in the WT conformation (**Fig. S3**) [30]. Using this methyl group as a probe, we determined the equilibrium constant K_{eq} (=[SLIP]/[WT]) at different pressures (20 to 2500 bar) by measuring the ratios of

299 the peak integrals corresponding to these two conformations (**Fig. 2B, C**). The SLIP
300 conformation was favored with increasing pressure up to ca. 1500 bar, at which point the
301 equilibrium constant appears to have converged. At 2500 bar, we observed the slow reduction of
302 signal intensities for both conformations over time, suggesting some kind of gradual instability
303 for the protein at the highest pressures.

304 From these data, we extracted the pressure dependence of K_{eq}, noting that it
305 monotonically increased until approximately 1500 bar. Beyond that pressure, we observed that it
306 remained approximately constant, showing that K_{eq} does not scale exponentially with pressure
307 and correspondingly that the free energy ΔG is not linearly dependent on pressure p (**Eq.1** and
308 **Fig. 2D**), necessitating the inclusion of a nonlinear term in compressibility. The plot was thus fit
309 for the differences in free energy between the two conformations at ambient pressure (referenced
310 to 1 bar, ΔG^0), volume (ΔV^0), and compressibility ($\Delta \beta V^0$) (**Eq. 3**). The SLIP conformation was
311 found to be 40.5 ml/mol smaller than the WT conformation, in reasonable agreement with the ca.
312 105 $Å^3$ (= 63 ml/mol) volume of internal cavities present uniquely in the WT conformation.
313 Additional support for the loss of these cavities came from the measurement that the WT
314 conformation was more compressible than the SLIP by 0.0285 ml/(mol bar). We attribute both
315 the volume and comparability differences to the collapse of internal cavities and increased
316 packing accompanying the WT to SLIP transition [29, 32].

317 **Pressure Jump Kinetic Analyses: WT and SLIP Interconvert by Transitioning into an**
318 **Intermediate State with Small Volume and Compressibility**

319 To complement the measurements above done under equilibrium pressure values, we
320 used pressure jump protocol for a series of kinetic analyses. To do so, we jumped the sample
321 pressure from 20 bar to various higher values, acquiring 1D ^{13}C-edited ^{1}H NMR spectra as the

322 system re-equilibrated, and measuring the populations of the two conformations by the area of
323 the respective L391 Hδ1 signals (**Fig. 3A**). Notably, we conducted these studies with
324 commercially-available instrumentation capable of completing even the largest of these jumps
325 within 30-60 sec., making it possible for us to perform the kinetic analyses due to the slow
326 kinetics of the interconversion process (**Fig. 3A**). Custom-built, NMR-compatible pressure
327 systems have recently been reported which are capable of such jumps approximately 100-fold
328 faster [23-24].

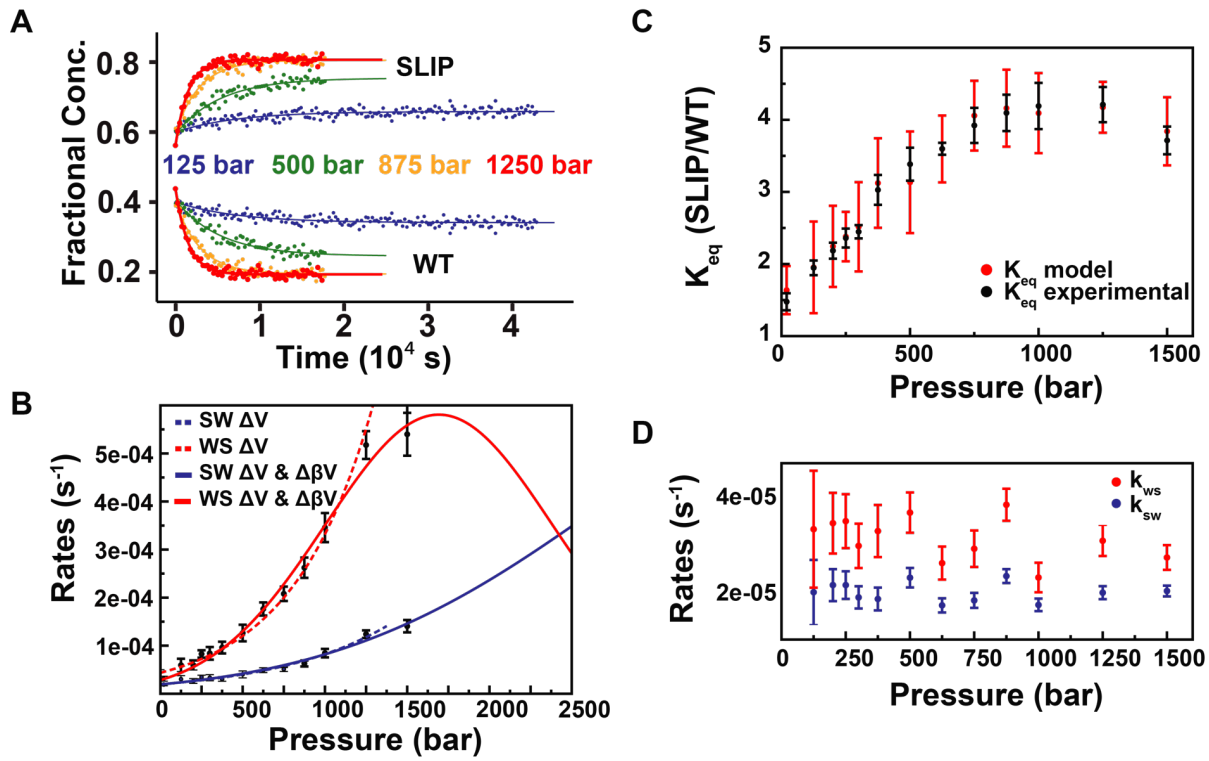

Figure 3. Kinetic analysis of the ARNT PAS-B interconversion. A) Examples of independent fits of the rate constants using the L391 Hδ1 ^{1}H methyl signals at the indicated pressures. Total population of the WT and SLIP was normalized to 1 for each analysis. B) Fitting of the decoupled rates (k_{sw} in blue, k_{ws} in red) as functions of pressure. Two models (without and with compressibility implemented) were used to fit the experimental data, using dashed (solid) lines to indicate fits without (with) compressibility included. C) Comparison of fit model (red) to experimental data (black). Equilibrium constants from the model are calculated from the rates derived from the kinetic analysis. D) Decoupled rates of relaxation. Each rate pair is plotted against the pressure the system was relaxed from. Relaxation rates appears to be independent of the initial pressure.

329 As an initial control of this approach, we extracted the K_{eq} values from these direct jump
330 experiments and fit them for the same parameters mentioned in the equilibrium analyses (**Fig.**
331 **S4**). This yielded a ΔV^0 of -46.1 ml/mol, and a $\Delta\beta V^0$ of -0.0433 ml/(mol bar) (**Table 1**). Direct
332 pressure jumps may induce convergence of K_{eq} at a slightly lower pressure (as indicated by the
333 bigger difference in compressibilities between the two states), but the overall trend remains
334 identical. In summary, we consistently found the SLIP conformation to be smaller and less
335 compressible than the WT conformation, as seen with the simpler equilibrium analyses.
336 Importantly, this also established that we did not need to be concerned with prior reports large
337 pressure jumps, ca. 10% of the protein's denaturing pressure, biasing the protein towards the
338 unfolded state [50].

Table 1. Summary of the kinetic and thermodynamic parameters derived from pressure-induced interconversion and unfolding of ARNT PAS-B variants

Thermodynamic Analyses		**Kinetic Analyses**	
SLIP – WT, step jumps[a]		**with ΔβV**	
ΔV^0 (ml/mol)	-40.5 ± 0.47	$\Delta V^{\ddagger}_{SW}$ (ml/mol)	-37.6 ± 3.0
ΔβV° (ml/(mol bar))	-0.0285 ± 0.00065	$\Delta V^{\ddagger}_{WS}$ (ml/mol)	-82.4 ± 7.4
SLIP – WT, direct jumps[b]		$\Delta\beta V^{\ddagger}_{SW}$ (ml/(mol bar))	-0.00875 ± 0.0034
ΔV^0 (ml/mol)	-46.1 ± 0.41	$\Delta\beta V^{\ddagger}_{WS}$ (ml/(mol bar))	-0.0487 ± 0.0066
ΔβV° (ml/(mol bar))	-0.0433 ± 0.00067	**without ΔβV**	
Unfolding (U - F)		$\Delta V^{\ddagger}_{SW}$ (ml/mol)	-32.8 ± 0.62
WT (ml/mol)	-126.3 ± 3.1	$\Delta V^{\ddagger}_{WS}$ (ml/mol)	-59.0 ± 1.38
TRIP (ml/mol)	-83.3 ± 2.3		

Uncertainties were estimated by bootstrapping. Random noises with mean of 0 and variance of the standard error were added to the raw data and fit repeatedly for n≥30 times to determine the 95% confidence interval. [a] step jumps – jumping pressure incrementally with 250 bar steps. [b] direct jumps – jumping pressure directly from 20 bar to various high pressures.

339 The intermediate state of ARNT PAS-B Y456T is only transiently visited during
340 interconversion [30], letting us assume that we could complement the prior equilibrium
341 measurements with kinetic analyses using a two-state model. As a first step of the analysis, we
342 established that the sum population of the two states remained constant at pressures below 2500
343 bar, implying the intermediate state did not accumulate during interconversion (**Fig. S5**). In the
344 two-state transition model, the apparent exchange rate is the sum of the two rate constants
345 corresponding to the transition from SLIP to WT and vice-versa (k_{sw} and k_{ws}) [51]. To obtain the
346 pressure dependence on both rates, we initially fit the apparent exchange rate vs. pressure to a
347 biexponential equation (**Eq. 4**), to yield the initial rates at 1 bar (k_{sw0} and k_{ws0}), the activation
348 volumes ($\Delta V_{sw}^{\ddagger}$ and $\Delta V_{ws}^{\ddagger}$), and the activation compressibilities ($\Delta\beta V_{sw}^{\ddagger}$ and $\Delta\beta V_{ws}^{\ddagger}$). However, this
349 equation requires simultaneous fitting of six parameters. Instead, we decoupled the two rates by
350 solving them numerically under different pressures using the differential equation pairs described
351 in Materials and Methods (**Eq. 5, 6**) and Supplementary Information (**Fig. S6, S7**). This allowed
352 us to independently fit each rate as a function of pressure with three parameters (**Eq. 7, 8**; **Fig.
353 3A, B**), summarized in **Table 1**. We observed negative activation volumes and compressibilities
354 for both transitions, implying that they proceed through an intermediate state which is smaller
355 and less compressible than the starting conformations. Moreover, the magnitude of the volume
356 barrier is bigger for the WT to SLIP transition, with a 44.8 ml/mol difference in activation
357 volumes, consistent with the volume difference obtained from the thermodynamic analysis (40.5
358 ml/mol). Taking the ratios of the two rate constants (k_{ws}/k_{sw}) at different pressures yielded
359 equilibrium constants matching experimental data (**Fig. 3C**). Since both activation volumes were
360 negative, the transition rates were correspondingly accelerated under pressure. The negative
361 activation compressibilities, on the other hand, suggest an unfolded transition state, as

362 replacement of interatomic contacts with hydration shells during unfolding will result in
363 significant compressibility reduction, as observed here [52]. Of note, as compressibility is small
364 and neglectable at lower pressures [18], we were able to fit the sub 1000 bar data points to a model
365 without compressibility, leading to the same observation that the SLIP conformation is smaller
366 than the WT conformation, albeit to a lesser extent (**Fig. 3B**; **Table 1**).

367 Unfolded proteins are generally smaller than their folded states [18, 20-21]. If the
368 interconversion of ARNT PAS-B Y456T truly goes through a chiefly unfolded intermediate
369 state, the activation volumes derived are expected to be comparable to the folding volumes of
370 similar sized (10-20 kDa) proteins. Indeed, the numbers are in good agreement with several other
371 proteins studied with pressure-dependent unfolding approaches, as summarized in **Table S1** [41, 53-
372 58]. Thus, the kinetic analyses further support our hypothesis.

373 **Pressure Induced Interconversion is Kinetically and Thermodynamically Reversible**

374 To validate the reversibility of the pressure-jump experiments, after equilibrating the
375 system under different pressures through direct pressure jumps, we relaxed the system from
376 higher pressures down to 20 bar and recorded ^{13}C-edited 1D ^{1}H NMR spectra during the
377 subsequent relaxation period. We extracted the two rate constants k_{ws} and k_{sw} during these times
378 and plotted them against the pressures prior to the relaxation (**Fig. 3D**). For all of the pressures
379 we used for extrapolating the rates (from 125 to 1500 bar), the relaxation rates remained the
380 same. The final equilibrium constants derived from these rates ([SLIP]/[WT]) were the same as
381 the initial 20 bar equilibrium constant the protein started with. This result, together with our
382 comparison of ^{15}N/^{1}H HSQC spectra recorded before and after pressure-jump experiments (**Fig.
383 S2**), implies that only the destination pressure determines the rate of interconversion, and that
384 this system is both thermodynamically and kinetically reversible up to at least 1500 bar.

385 We previously characterized the temperature dependence of the ARNT PAS-B Y456T
386 interconversion process by monitoring the rates of interconversion from the SLIP to the WT
387 conformation at different temperatures after chromatographic separation of the two forms [29-30].
388 To conclude our reversibility check, we tested if the same temperature dependence of the protein
389 still holds true following pressure-jump experiments. We equilibrated the protein at 1000 bar at
390 four different temperatures (278.1, 283.1, 288.1, and 291.1K) to mimic the equilibrium
391 perturbation of the previous work, where the SLIP conformation dominated [30]. Following this,
392 we relaxed the system to 20 bar and recorded ^{13}C-edited 1D ^{1}H NMR spectra during relaxation
393 and extracted the apparent exchange rates from SLIP to WT by fitting the time-dependent
394 equilibrium constants to single exponential decay curves (**Fig. S8**). This allowed us to derive the
395 entropy and enthalpy of activation by fitting the rates to the Eyring equation. The extracted
396 entropic (-47.8 cal/(mol degree), or -14.2 kcal/mol at 298K) and enthalpic (7.4 kcal/mol)
397 contributions to the activation energy are similar to those obtained from our previous study [30].
398 We interpret the large entropic barrier for the interconversion as the result of non-polar residues
399 that are exposed during the unfolded transition state [30], further supporting our pressure analysis
400 that the intermediate state is mostly unfolded. These results also imply the relaxation process we
401 monitored here after pressure perturbation is the same as the interconversion process that we
402 previously observed with chromatographic separation [29-30], suggesting that we are observing a
403 common process despite differences in the type of initial perturbation.

404 **Activation Volumes of the ARNT PAS-B Y456T are Comparable to the Unfolding Volumes**
405 **of the WT and TRIP Variant Detected by Pressure Jump NMR**

406 To better characterize the transition state conformation of ARNT PAS-B Y456T, we
407 compared its activation volumes of interconversion to the unfolding volumes of the two starting

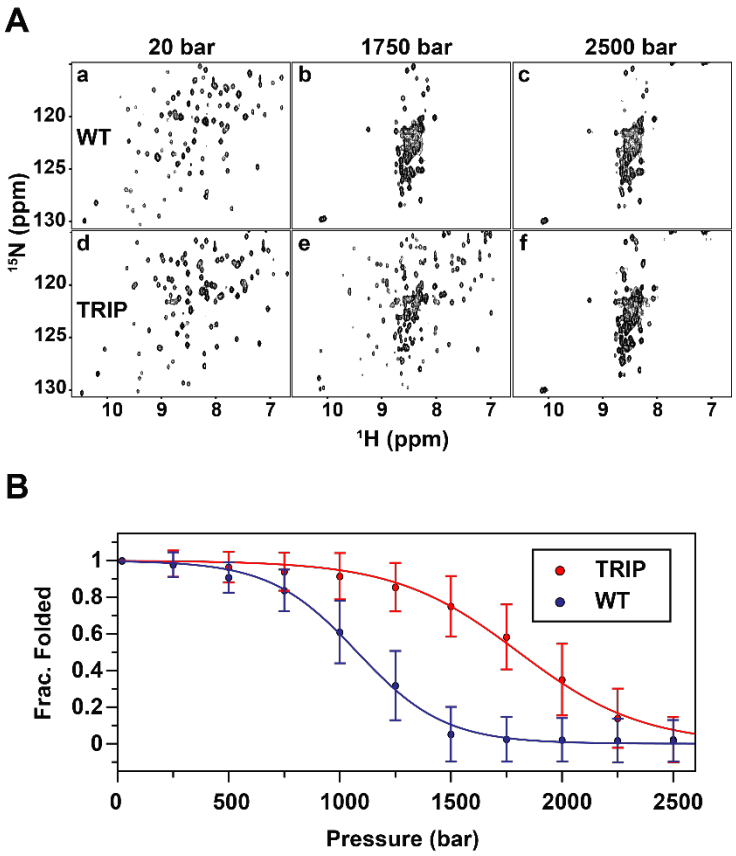

Figure 4. Unfolding profile of ARNT PAS-B WT and TRIP mutant detected by high-pressure NMR ^{15}N/^{1}H HSQC at 278 K and 3.0 M urea. A) Example ^{15}N/^{1}H-HSQC spectra of WT and TRIP at different pressures. (a-c) NMR spectra of WT at initial pressure (20 bar), intermediate pressure (1750 bar), and final pressure (2500 bar). (d-f) NMR spectra of TRIP mutant. B) Average unfolding curves for ARNT PAS-B WT and TRIP mutant. Peak intensities are normalized between 0 and 1.

408 points, the WT and SLIP conformations, as adopted by the WT and TRIP variant, respectively.
409 As neither protein substantially unfolded within our experimentally-accessible pressure range (≤
410 2500 bar), we added 3 M urea to slightly lower the stability of both samples. From ^{15}N/^{1}H HSQC
411 spectra we acquired at different pressures in the presence of denaturant, it was clear that all the
412 resolved backbone peaks showed pressure-induced reductions in intensity, with no obvious peak
413 broadening (**Fig. S9**). This was accompanied by the appearance of intense peaks with sharp
414 linewidths and poor ^{1}H chemical shift dispersion, consistent with pressure-induced protein
415 unfolding. The protein appeared to be completely unfolded at approximately 1750 bar for WT

and 2500 bar for the TRIP variant (**Fig. 4A, S9**). By fitting the protein unfolding curves for both the WT and the TRIP variant to a two-state model (**Eq. 10**, **Fig. 4B**), we could extract two key parameters: the average volume difference between the folded and the unfolded protein (ΔV_f) and the free energy of folding (ΔG_f^0) [20, 59]. The folding energy and volumes of both WT and TRIP mutant are recorded in **Table 1**. The unfolding volumes indicate a 43.0 ml/mol difference between the two folded structures, and the folding energies predict a 2.7:1 ratio between the SLIP and the WT conformation at ambient pressure, both similar to what we have observed for the ARNT PAS-B Y456T (40.5 ml/mol and 1.5:1, respectively), suggesting these values are faithful estimations. The activation volumes of the ARNT PAS-B Y456T, which represent the volume differences between the two folded states to the intermediate state, are smaller but comparable to the unfolding volumes of the WT and TRIP variant (-82.4 ml/mol vs. -126.3 ml/mol for WT, -37.6 ml/mol vs. -83.3 ml/mol for SLIP), reaffirming that the interconversion

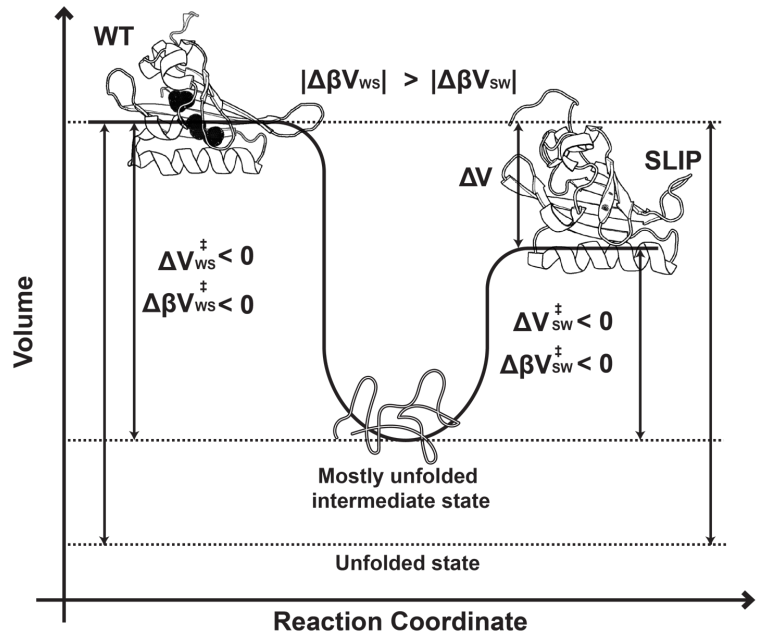

Figure 5. Comparison between the folded and unfolded states of ARNT PAS-B Y456T. Schematic representation comparing the folded, intermediate, and unfolded states of ARNT PAS-B Y456T. Measurement of the volumes and compressibilities are recorded in **Table 1**.

428 intermediate state of ARNT PAS-B Y456T is partially unfolded. A schematic figure describing
429 the relationships among the two folded conformations, the intermediate state, and the unfolded
430 state is shown in **Fig. 5**.

431 **Pressure-induced Nonlinear Chemical Shift Changes and Residue Compressibilities Predict**
432 **Cavity Locations**

433 Certain types of pressure-induced NMR chemical shift changes have been related to
434 conformational changes within proteins [26-27]. The changes in ^{15}N and ^{13}C, and to a lesser extent
435 ^{1}H, chemical shifts can be fit to a function of pressure with a linear and a nonlinear term (**Eq. 11**)
436 [18]. Of particular interest structurally is the nonlinear coefficient (c_i) of the backbone amide ^{15}N
437 and ^{1}H nuclei, where larger values are particularly sensitive on the ability of proteins to visit
438 multiple conformational states upon application of pressure. Such information can be analyzed in
439 bulk, with larger average c_i values or broader c_i distributions reflecting the presence of internal
440 cavities or voids which enable protein flexibility with increased pressure [18, 26, 28, 47]. At a residue-
441 specific level, larger c_i values are likely associated with residues located near the internal cavities
442 of a protein [18, 28].

443 To test if this holds true for the WT and SLIP conformations of ARNT PAS-B, we
444 acquired ^{15}N/^{1}H HSQC spectra of both WT and TRIP samples of ARNT PAS-B at pressures up
445 to 2000 bar (**Fig. 6A**). We fit the pressure-dependent changes in ^{15}N chemical shifts of
446 assignable residues to **Eq. 11**, using these to extract the ^{15}N c_i values for both conformations
447 (**Fig. 6B**) [29, 31]. While the two conformers have similar overall structures, we observed markedly
448 different distributions of the backbone amide ^{15}N c_i values. Specifically, we observed a global
449 reduction of the magnitude of c_i in the SLIP conformation, supporting the view that it has
450 reduced internal void volume and flexibility compared to the WT conformation. We calculated

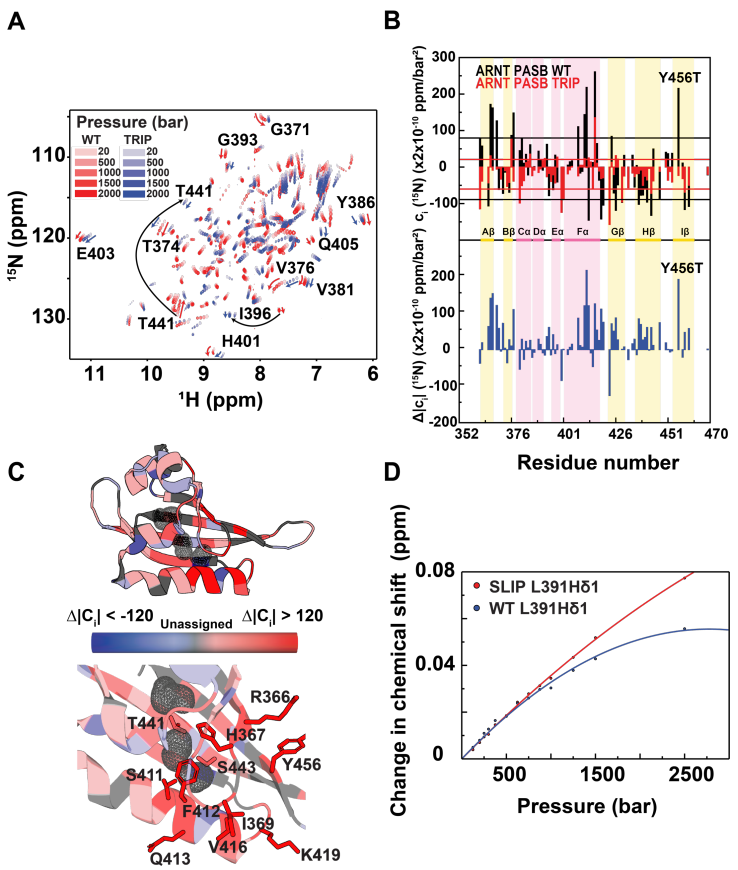

Figure 6. Residues surrounding cavities of ARNT PAS-B are rigidified in the SLIP conformation. A) ^{15}N/^{1}H HSQC spectra of WT and TRIP variant ARNT PAS-B under pressures from 20 to 2000 bar, showing large chemical shift differences between conformations despite high structural similarities between the two. Pressure-dependent non-linear chemical shift changes are also different between WT and SLIP, which are highlighted by red and blue arrows for several example residues. B) Pressure-dependent non-linear chemical shift changes of the two conformations as measured by ^{15}N c_i (top panel) and differences in non-linearities between the two conformations (|WT c_i|-|SLIP c_i|) (bottom panel) mapped onto the sequence and secondary structure of WT ARNT PAS-B. The standard deviation of WT c_i (black lines, 84 $\times 2\times 10^{-10}$ ppm/bar^2) is about 2 times the standard deviation of SLIP c_i (red lines, 41 $\times 2\times 10^{-10}$ ppm/bar^2). C) Mapping the residue-specific differences in non-linear coefficients between WT and SLIP suggest that WT is globally more dynamic. Residues with large non-linear coefficient differences ($\Delta c_i > 120$) between WT and SLIP (366, 367, 369, 411, 412, 413, 416, 419, and 456) are located near the cavities (gray mesh) or on loop regions of WT ARNT PAS-B. Other residues oriented toward cavities (i.e. T441 and S443) also show more non-linear chemical shift changes in WT than SLIP. d) ^{1}H chemical shift changes of L391 Hδ1 for both the WT and SLIP conformations of ARNT PAS-B Y456T are plotted against pressure. The chemical shift change of the residue in the WT conformation shows remarkably more non-linear characteristic than it is in the SLIP conformation.

the differences in nonlinear coefficients by subtracting the absolute values of c_i of the SLIP conformation from the WT conformation (**Eq. 12**). Residues with the largest ^{15}N c_i differences were located near the internal cavities or on loop regions of the WT structure (**Fig. 6C**). Notably, many of these residues contribute to the formation of the cavities in the WT ARNT PAS-B [32].

455 The cavities apparently collapse in the SLIP conformation due to the +3 shift and inversion of
456 the Iβ-strand, explaining the significant c_i reduction of these residues in the SLIP conformation.
457 Interestingly, residue Y456, the site of the Y456T point mutation that creates the SLIP
458 conformation, has one of the largest ^{15}N c_i difference between the two conformations.

459 We also suspect that the residue-specific compressibility also depends on whether the
460 residue is near a cavity. As expected, when we fit the ^{1}H chemical shift of L391 δ1 to **Eq. 11** to
461 extract c_i, we obtained a larger nonlinear coefficient for the peak corresponding to the WT
462 conformation compared to the SLIP conformation (**Fig. 6D**), matching the compressibility
463 difference observed between the two states, confirming our speculation. We also compared the
464 pressure-dependent response of several other methyl peaks corresponding to the WT and SLIP
465 conformation using the ^{13}C/^{1}H-HSQC spectra of ARNT PAS-B Y456T (**Fig. S10**). We found
466 several cavity-oriented methyl groups to have larger c_i values for the WT conformation in H
467 and/or C dimension(s) (L391 δ2, I396 δ1, L408 δ1 and δ2, and M439 ε1). Correspondingly, their
468 pressure dependent K_{eq} shifts (from WT to SLIP) were also slowed down at higher pressures as
469 the result of negative compressibility changes, consistent with our analysis of L391 δ1. The c_i
470 values for another residue near the cavity, V384 γ1, was similar between the two conformations.
471 This can potentially be attributed to the smaller local void volume difference between the states,
472 as V384 is next to a loop and close to a solvent exposed opening in both structures.

473 These data suggest the pressure-dependent nonlinear chemical shift changes may be
474 related to the local compressibility of the protein, and both of which can help with the
475 identification of cavity sites. This is in line with the prior notion that larger compressibility is
476 correlated with larger volume fluctuations, which are generally observed near cavities, where
477 residues are less tightly packed [60].

478 **DISCUSSION**

479 Studying the reversible interconversions of proteins between multiple folded
480 conformations has always been an intriguing topic [8-9, 61-63]. While several techniques are
481 available for probing and characterizing such transitions, there is an unfortunate lack of
482 streamlined methods to easily and reversibly manipulate conformational changes [11, 13]. There has
483 been significant interest in pressure-variable experiments recently, as pressure change can be
484 used to shift equilibria between protein conformations of different volumes [18, 26, 38, 62, 64-65]. While
485 earlier works on pressure-induced protein transitions rely mostly on Trp fluorescence
486 measurement [58], the availability of commercial NMR-compatible high-pressure equipment
487 enables a broader range of site-specific experiments. Previous studies using high-pressure NMR
488 heavily emphasize the characterization of folding and unfolding transitions of proteins in the
489 kbar range [18, 20-21, 24, 26, 54, 59]. Lower pressures (i.e. under 1000 bar) have been shown to populate
490 alternative states of proteins [18, 26], but detailed kinetic characterizations of such processes have
491 been difficult as the timescale of the transitions are typically faster than the time it takes for
492 pressure jumps to stabilize and outside the accessible time resolution of many NMR experiments
493 [23-24, 65]. Using the slowly-interconverting ARNT PAS-B Y456T as a test case, we here
494 demonstrate pressure-jump NMR as a tool to manipulate, monitor, and characterize the
495 interconversion of a protein between stably folded conformations.

496 ARNT PAS-B Y456T exists in two conformations, the native-like WT conformation and
497 the SLIP conformation that shifts and inverts the central Iβ-strand, accompanied by
498 isomerization of the nearby N448-P449 peptide bond [29]. We previously investigated the
499 interconversion between these two conformations using kinetic measurements of the re-
500 establishment of equilibrium following perturbation by chromatographic isolation of one

501 conformer. Coupled with stopped-flow fluorescence protein (un)folding measurements [29-30], we
502 proposed the ARNT PAS-B Y456T likely switches conformers through a chiefly unfolded
503 intermediate state. This model was primarily supported by two lines of evidence [30]: 1). The
504 transition requires 15 out of the 26 inter-strand backbone hydrogen bonds on the β-sheet to be
505 reformed during the transition (**Fig. S11**), representing a very energetically unfavored process;
506 2). kinetic studies revealed similar unfolding and transition rates. However, we could not directly
507 probe the difference between the folded and the transition states, and the process of manipulating
508 protein equilibrium was particularly challenging. With pressure jump NMR experiments, we
509 successfully shifted the equilibrium between the two conformations. By examining the relaxation
510 rates and their temperature dependence, we found that pressure-perturbed equilibrium changes of
511 ARNT PAS-B Y456T were remarkably reversible, making it a much faster and more reliable
512 approach than the chromatographic isolation we previously implemented. We also
513 thermodynamically and kinetically characterized the interconversion process, with strong
514 emphasis on quantifying volume and compressibility differences among the WT, SLIP, and the
515 intermediate states, which are parameters not accessible through other techniques, underscoring
516 the broader applications of pressure-jump NMR technique for studying protein conformational
517 changes.

518 There is a consensus that the molar volume of an unfolded protein is smaller than that of
519 its folded state [18, 20, 54, 59]. In this context, it is not surprising that the activation volumes of
520 transition from WT to SLIP and vice versa are negative. The combined size of two major cavities
521 of WT ARNT PAS-B was 105 $Å^3$ (**Fig. 1**), with the total cavity volume estimated to be ca. 105-
522 150 $Å^3$ [32]. In contrast, SLIP does not have any cavities [29]. Interestingly, the activation volume for
523 the WT to SLIP transition (-82.4 ml/mol, or 137 $Å^3$/molecule) is strikingly similar to the cavity

524 size of the WT conformation. The SLIP to WT transition, in contrast, requires a much smaller
525 activation volume (**Table 1**). While the pressure-induced volume change of a system is a
526 combined effect from compressing both protein and solvent [20], we found a positive correlation
527 between cavity size and activation volume. We can now postulate the transition between the two
528 confirmations require the protein to collapse its internal cavities and voids to reduce its total
529 volume, consistent with a transition from a folded to an unfolded state. This claim is further
530 supported by Roche *et al.*'s [54] recent work highlighting that pressure driven protein unfolding is a
531 result of cavity elimination.

532 Unlike most biophysical studies of proteins exposed to high pressure, where
533 compressibility is assumed to be constant [18, 20], our analyses revealed substantial compressibility
534 differences between the two conformations adopted by ARNT PAS-B Y456T. This result
535 initially surprised us, as compressibility is typically not a significant contributor to the change in
536 free energy, ΔG for pressures below 2000 bar [18]. This contradicts with our observations, as the
537 pressure dependence of the WT to SLIP transition dramatically weakened at higher pressures,
538 resulting in a K_{eq} plateau at ca. 1750 bar. As described above, we successfully incorporated a
539 compressibility term for ΔG calculation (**Eq. 3**) [18], letting us better estimate ΔG up to 1750 bar.
540 We posit that this compressibility difference reflects changes in packing, hydration, and cavity
541 size between the two conformations (**Fig. 1**) [29, 32, 52], which are probed in this work by
542 monitoring the cavity-lining residue L391 (**Fig. S3**). Of note, by using the first three terms of the
543 Taylor series (**Eq. 2**), our model is only valid for a pressure range. Following the collapse of the
544 cavities in the WT conformation, which we estimate to happen at mid-1600 bar based on the
545 cavity size, its compressibility will drop sharply [66], bringing the value close to that of the SLIP

546 conformation. It is therefore unsurprising that the experimental K_{eq} values deviated from our
547 model at higher pressures.

548 Building on the need to include compressibility differences for the equilibrium analyses,
549 we similarly included activation compressibilities ($\Delta\beta V_{ws}^{\ddagger}$ and $\Delta\beta V_{sw}^{\ddagger}$) in our kinetic analyses
550 (**Eq. 4**). These values represent the differences in compressibility between the respective ground
551 state conformers and the transition state between them, and the fact that both values are negative
552 supports the hypothesis that interconversion proceeds through a highly unfolded intermediate, as
553 compressibility is inversely correlated with a protein's degree of unfolding [60]. Lastly, we note
554 that we did not include compressibility changes for the unfolding analysis of ARNT PAS-B WT
555 and TRIP, given that these were based on global averages of signals (> 60 residues) distributed
556 throughout both proteins which we assume to average out contributions from sites near cavities
557 (compressibility-dependent) and those far from cavities (compressibility-independent) [18, 28].

558 Finally, pressure-induced chemical shift changes are routinely analyzed by separating
559 components which are linearly- and nonlinearly-dependent on pressure [18, 21] (**Eq. 11**). While the
560 linear responses are relatively invariant among proteins, work from our lab and others has
561 established that the nonlinear responses are attributed to shifts among low-lying sub-states of the
562 protein that are populated under high pressure [26-28]. We demonstrate that the WT conformation
563 has more nonlinear chemical shift changes globally compared to the SLIP conformation, and
564 larger differences could be clustered into two regions, between Aβ and Bβ, Fβ and Gβ (**Fig. 6B**).
565 Intriguingly, the same clusters of residues are in the vicinity of the cavities observed in prior
566 ARNT PAS-B structures, and have been associated with the binding of KG-548, a moderate-
567 affinity compound known to bind to ARNT PAS-B and disrupt the interactions between ARNT
568 PAS-B and TACC3 co-activator [32]. Since the SLIP conformation does not contain any cavities,

569 the same residues are likely to be more packed and therefore lose their dynamics, thus reducing
570 the pressure-dependent volume fluctuation [67]. The reduction in pressure-induced nonlinear
571 chemical shift changes of the TRIP variant seems to be a readout of this difference. Intuitively,
572 this is because residues near cavities have more space to sample multiple conformations upon
573 compression, resulting in structural fluctuations of the protein between sub-states in the fast
574 regime on the NMR timescale [18, 26]. Since both nonlinear chemical shift changes and
575 compressibility probe for the volume-dependent local environment a residue resides in,
576 measuring the nonlinear coefficient of chemical shift changes and compressibility can go hand-
577 in-hand for more accurate characterization of cavities in proteins (as has been linked
578 mathematically in the past [68]). Remarkably, the cavities in the WT ARNT PAS-B were not
579 initially observed in the solution structure [31], showing the potential of pressure-NMR as the
580 means of rapidly identifying smaller cavities from moderate resolution structures where cavities
581 and/or ligand binding pockets are not obvious [31].

582 **CONCLUSION**

583 The shift of the β-strand register at an interaction interface enabled by a single point
584 mutation is mechanistically intriguing and raises fundamental questions about the relative
585 stabilities of the ground state and energetically close alternate conformers [30, 69-70]. Using 1D and
586 2D pressure-jump NMR experiments, we examined one such case by elucidating the volume and
587 compressibility differences between two stably folded conformations of ARNT PAS-B which
588 interconvert when enabled by a single point mutation, Y456T. We demonstrated that the
589 wildtype (WT) state has a substantially larger internal volume and compressibility compared to
590 the alternate slip conformation (SLIP), and that these differences are largely attributed to the
591 cavities unique to the WT state. Furthermore, we show that the transition of ARNT PAS-B

592 between the two states requires it to go through an intermediate state that is smaller in volume
593 and compressibility than both folded conformations, supporting the hypothesis that this is a
594 chiefly unfolded transition state. Additionally, we found that the residue-specific compressibility
595 and nonlinear chemical shift responses to pressure can be used to predict whether residues are
596 located close to cavities. In summary, we have shown how varying pressure can be easily applied
597 to reversibly shift the equilibrium of a protein between two stably folded conformations, letting
598 us characterize structural and thermodynamic information otherwise difficult to access [20]. We
599 believe that this approach can be applied to other proteins which undergo large scale
600 conformational changes, particularly with recent instrumentation advances that allow
601 millisecond-timescale pressure jumps [23-24]. We anticipate that such studies will be particularly
602 useful studying systems where protein flexibility is essential, including enzymatic
603 conformational changes, protein/ligand interactions, and metamorphic systems [9-11].

604 **SUPPLEMENTARY INFORMATION**

605 **Table S1.** Unfolding Volumes of Proteins with Similar Size as ARNT PAS-B.

606 **Figure S1.** Overlaid $^{15}N/^{1}H$ and $^{13}C/^{1}H$ HSQC spectra of ARNT PAS-B Y456T recorded as a
607 function of pressure.

608 **Figure S2.** Comparison of $^{15}N/^{1}H$ and $^{13}C/^{1}H$ HSQC spectra recorded at 20 bar pre- and post-
609 pressure-jump NMR experiments.

610 **Figure S3.** Structural differences between the WT and SLIP conformation of ARNT.

611 **Figure S4.** Equilibrium constant of ARNT PAS-B Y456T (SLIP/WT) fitted as a function of
612 pressure.

613 **Figure S5.** Fluctuation of the total population of the WT and SLIP conformations at different
614 pressures.

Figure S6. Numerical solutions to rate equations under pressure.

Figure S7. Estimation of the parameter uncertainty.

Figure S8. Temperature dependence of ARNT PAS-B Y456T interconversion between the SLIP and WT conformations

Figure S9. $^{15}N/^{1}H$ HSQC spectra of ARNT PAS-B WT and TRIP mutant under pressure at 278 K and 3.0 M urea.

Figure S10. Pressure-dependent chemical shift changes and equilibrium constants (SLIP/WT) of cavity-oriented residues of ARNT PAS-B Y456T.

Figure S11. Hydrogen bonds between Iβ strand and adjacent Hβ and Aβ strands of the WT and SLIP conformations.

AUTHOR CONTRIBUTION

X.X, D.G, J.M.A, and K.H.G designed the experiments; X.X, J.M.A, and D.G performed the experiments; X.X and K.H.G. analyzed the data and wrote the manuscript.

FUNDING SOURCES

This work was supported by NSF grant MCB 1818148

ACKNOWLEDGMENT

We thank members of the Gardner laboratory for constructive comments.

COMPETING INTERESTS

The authors declare no competing interests.

634 **REFERENCES**

635 (1) Leopold, P. E.; Montal, M.; Onuchic, J. N., Protein folding funnels: a kinetic approach to
636 the sequence-structure relationship. *Proc Natl Acad Sci U S A* **1992,** *89* (18), 8721-8725.

637 (2) Onuchic, J. N.; Nymeyer, H.; Garcia, A. E.; Chahine, J.; Socci, N. D., The energy
638 landscape theory of protein folding: insights into folding mechanisms and scenarios. *Adv Protein*
639 *Chem* **2000,** *53*, 87-152.

640 (3) Ishikawa, H.; Kwak, K.; Chung, J. K.; Kim, S.; Fayer, M. D., Direct observation of fast
641 protein conformational switching. *Proc Natl Acad Sci U S A* **2008,** *105* (25), 8619-8624.

642 (4) Tuinstra, R. L.; Peterson, F. C.; Kutlesa, S.; Elgin, E. S.; Kron, M. A.; Volkman, B. F.,
643 Interconversion between two unrelated protein folds in the lymphotactin native state. *Proc Natl*
644 *Acad Sci U S A* **2008,** *105* (13), 5057-5062.

645 (5) Ha, J. H.; Loh, S. N., Protein conformational switches: from nature to design. *Chemistry*
646 **2012,** *18* (26), 7984-7999.

647 (6) Zoltowski, B. D.; Schwerdtfeger, C.; Widom, J.; Loros, J. J.; Bilwes, A. M.; Dunlap, J. C.;
648 Crane, B. R., Conformational switching in the fungal light sensor Vivid. *Science* **2007,** *316*
649 (5827), 1054-1057.

650 (7) Harper, S. M.; Neil, L. C.; Gardner, K. H., Structural basis of a phototropin light switch.
651 *Science* **2003,** *301* (5639), 1541-1544.

652 (8) London, R. E., HIV-1 Reverse Transcriptase: A Metamorphic Protein with Three Stable
653 States. *Structure* **2019,** *27* (3), 420-426.

654 (9) Murzin, A. G., Biochemistry. Metamorphic proteins. *Science* **2008,** *320* (5884), 1725-
655 1726.

656 (10) Yadid, I.; Kirshenbaum, N.; Sharon, M.; Dym, O.; Tawfik, D. S., Metamorphic proteins
657 mediate evolutionary transitions of structure. *Proc Natl Acad Sci U S A* **2010,** *107* (16), 7287-
658 7292.
659 (11) Agarwal, P. K.; Doucet, N.; Chennubhotla, C.; Ramanathan, A.; Narayanan, C.,
660 Conformational Sub-states and Populations in Enzyme Catalysis. *Methods Enzymol* **2016,** *578*,
661 273-297.
662 (12) Brereton, A. E.; Karplus, P. A., Native proteins trap high-energy transit conformations.
663 *Sci Adv* **2015,** *1* (9), e1501188.
664 (13) Loria, J. P.; Berlow, R. B.; Watt, E. D., Characterization of enzyme motions by solution
665 NMR relaxation dispersion. *Acc Chem Res* **2008,** *41* (2), 214-221.
666 (14) Alderson, T. R.; Kay, L. E., Unveiling invisible protein states with NMR spectroscopy.
667 *Curr Opin Struct Biol* **2020,** *60*, 39-49.
668 (15) Scheuermann, T. H.; Tomchick, D. R.; Machius, M.; Guo, Y.; Bruick, R. K.; Gardner, K.
669 H., Artificial ligand binding within the HIF2alpha PAS-B domain of the HIF2 transcription
670 factor. *Proc Natl Acad Sci U S A* **2009,** *106* (2), 450-455.
671 (16) Di Russo, N. V.; Estrin, D. A.; Marti, M. A.; Roitberg, A. E., pH-Dependent
672 conformational changes in proteins and their effect on experimental pK(a)s: the case of
673 Nitrophorin 4. *PLoS Comput Biol* **2012,** *8* (11), e1002761.
674 (17) Caldwell, C. R., Temperature-Induced Protein Conformational Changes in Barley Root
675 Plasma Membrane-Enriched Microsomes: II. Intrinsic Protein Fluorescence. *Plant Physiol* **1987,**
676 *84* (3), 924-929.
677 (18) Akasaka, K., Probing conformational fluctuation of proteins by pressure perturbation.
678 *Chem Rev* **2006,** *106* (5), 1814-1835.

679 (19) Caro, J. A.; Wand, A. J., Practical aspects of high-pressure NMR spectroscopy and its
680 applications in protein biophysics and structural biology. *Methods* **2018,** *148*, 67-80.
681 (20) Roche, J.; Royer, C. A., Lessons from pressure denaturation of proteins. *J R Soc*
682 *Interface* **2018,** *15* (147).
683 (21) Akasaka, K.; Kitahara, R.; Kamatari, Y. O., Exploring the folding energy landscape with
684 pressure. *Arch Biochem Biophys* **2013,** *531* (1-2), 110-115.
685 (22) Liu, Y.; Prigozhin, M. B.; Schulten, K.; Gruebele, M., Observation of complete pressure-
686 jump protein refolding in molecular dynamics simulation and experiment. *J Am Chem Soc* **2014,**
687 *136* (11), 4265-4272.
688 (23) Charlier, C.; Alderson, T. R.; Courtney, J. M.; Ying, J.; Anfinrud, P.; Bax, A., Study of
689 protein folding under native conditions by rapidly switching the hydrostatic pressure inside an
690 NMR sample cell. *Proc Natl Acad Sci U S A* **2018,** *115* (18), E4169-E4178.
691 (24) Charlier, C.; Courtney, J. M.; Alderson, T. R.; Anfinrud, P.; Bax, A., Monitoring (15)N
692 Chemical Shifts During Protein Folding by Pressure-Jump NMR. *J Am Chem Soc* **2018,** *140*
693 (26), 8096-8099.
694 (25) Fuglestad, B.; Stetz, M. A.; Belnavis, Z.; Wand, A. J., Solution NMR investigation of the
695 response of the lactose repressor core domain dimer to hydrostatic pressure. *Biophys Chem* **2017,**
696 *231*, 39-44.
697 (26) Akasaka, K.; Li, H., Low-lying excited states of proteins revealed from nonlinear
698 pressure shifts in 1H and 15N NMR. *Biochemistry* **2001,** *40* (30), 8665-8671.
699 (27) Williamson, M. P.; Kitahara, R., Characterization of low-lying excited states of proteins
700 by high-pressure NMR. *Biochim Biophys Acta Proteins Proteom* **2019,** *1867* (3), 350-358.

701 (28) Gagné, D. A., R.; Edupuganti, U.R.; Williams, J.; Aramini, J.M.; Akasaka, K., Gardner,
702 K.H. , Use of high pressure NMR spectroscopy to rapidly identify internal ligand-binding voids
703 in proteins. Manuscript under review. **2020**.
704 (29) Evans, M. R.; Card, P. B.; Gardner, K. H., ARNT PAS-B has a fragile native state
705 structure with an alternative beta-sheet register nearby in sequence space. *Proc Natl Acad Sci U*
706 *S A* **2009,** *106* (8), 2617-2622.
707 (30) Evans, M. R.; Gardner, K. H., Slow transition between two beta-strand registers is
708 dictated by protein unfolding. *J Am Chem Soc* **2009,** *131* (32), 11306-11307.
709 (31) Card, P. B.; Erbel, P. J.; Gardner, K. H., Structural basis of ARNT PAS-B dimerization:
710 use of a common beta-sheet interface for hetero- and homodimerization. *J Mol Biol* **2005,** *353*
711 (3), 664-677.
712 (32) Guo, Y.; Partch, C. L.; Key, J.; Card, P. B.; Pashkov, V.; Patel, A.; Bruick, R. K.;
713 Wurdak, H.; Gardner, K. H., Regulating the ARNT/TACC3 axis: multiple approaches to
714 manipulating protein/protein interactions with small molecules. *ACS Chem Biol* **2013,** *8* (3), 626-
715 635.
716 (33) Wu, D.; Potluri, N.; Lu, J.; Kim, Y.; Rastinejad, F., Structural integration in hypoxia-
717 inducible factors. *Nature* **2015,** *524* (7565), 303-308.
718 (34) Guo, Y.; Scheuermann, T. H.; Partch, C. L.; Tomchick, D. R.; Gardner, K. H., Coiled-
719 coil coactivators play a structural role mediating interactions in hypoxia-inducible factor
720 heterodimerization. *J Biol Chem* **2015,** *290* (12), 7707-7721.
721 (35) Wu, D.; Su, X.; Potluri, N.; Kim, Y.; Rastinejad, F., NPAS1-ARNT and NPAS3-ARNT
722 crystal structures implicate the bHLH-PAS family as multi-ligand binding transcription factors.
723 *Elife* **2016,** *5*.

724 (36) Partch, C. L.; Card, P. B.; Amezcua, C. A.; Gardner, K. H., Molecular basis of coiled coil
725 coactivator recruitment by the aryl hydrocarbon receptor nuclear translocator (ARNT). *J Biol*
726 *Chem* **2009,** *284* (22), 15184-15192.
727 (37) Partch, C. L.; Gardner, K. H., Coactivators necessary for transcriptional output of the
728 hypoxia inducible factor, HIF, are directly recruited by ARNT PAS-B. *Proc Natl Acad Sci U S A*
729 **2011,** *108* (19), 7739-7744.
730 (38) Collins, M. D.; Kim, C. U.; Gruner, S. M., High-pressure protein crystallography and
731 NMR to explore protein conformations. *Annu Rev Biophys* **2011,** *40*, 81-98.
732 (39) Matthews, B. W., Proteins under pressure. *Proc Natl Acad Sci U S A* **2012,** *109* (18),
733 6792-6793.
734 (40) Mozhaev, V. V.; Heremans, K.; Frank, J.; Masson, P.; Balny, C., High pressure effects
735 on protein structure and function. *Proteins* **1996,** *24* (1), 81-91.
736 (41) Rouget, J. B.; Aksel, T.; Roche, J.; Saldana, J. L.; Garcia, A. E.; Barrick, D.; Royer, C.
737 A., Size and sequence and the volume change of protein folding. *J Am Chem Soc* **2011,** *133* (15),
738 6020-6027.
739 (42) Quinlan, R. J.; Reinhart, G. D., Baroresistant buffer mixtures for biochemical analyses.
740 *Anal Biochem* **2005,** *341* (1), 69-76.
741 (43) Johnson, B. A., From Raw Data to Protein Backbone Chemical Shifts Using NMRFx
742 Processing and NMRViewJ Analysis. *Methods Mol Biol* **2018,** *1688*, 257-310.
743 (44) Norris, M.; Fetler, B.; Marchant, J.; Johnson, B. A., NMRFx Processor: a cross-platform
744 NMR data processing program. *J Biomol NMR* **2016,** *65* (3-4), 205-216.

745 (45) Elzhov, T. V. M., K. M.; Spiess, A.; Bolker, B., minpack.lm: R Interface to the
746 Levenberg-Marquardt Nonlinear Least-Squares Algorithm Found in MINPACK, Plus Support
747 for Bounds. R package version 1.2-1. https://CRAN.R-project.org/package=minpack.lm. **2006**.
748 (46) Fossat, M. J.; Dao, T. P.; Jenkins, K.; Dellarole, M.; Yang, Y.; McCallum, S. A.; Garcia,
749 A. E.; Barrick, D.; Roumestand, C.; Royer, C. A., High-Resolution Mapping of a Repeat Protein
750 Folding Free Energy Landscape. *Biophys J* **2016,** *111* (11), 2368-2376.
751 (47) Akasaka, K.; Li, H.; Yamada, H.; Li, R.; Thoresen, T.; Woodward, C. K., Pressure
752 response of protein backbone structure. Pressure-induced amide 15N chemical shifts in BPTI.
753 *Protein Sci* **1999,** *8* (10), 1946-1953.
754 (48) Scheuermann, T. H.; Li, Q.; Ma, H. W.; Key, J.; Zhang, L.; Chen, R.; Garcia, J. A.;
755 Naidoo, J.; Longgood, J.; Frantz, D. E.; Tambar, U. K.; Gardner, K. H.; Bruick, R. K., Allosteric
756 inhibition of hypoxia inducible factor-2 with small molecules. *Nat Chem Biol* **2013,** *9* (4), 271-
757 276.
758 (49) Chen, C. R.; Makhatadze, G. I., ProteinVolume: calculating molecular van der Waals and
759 void volumes in proteins. *BMC Bioinformatics* **2015,** *16*, 101.
760 (50) Roche, J.; Royer, C. A.; Roumestand, C., Exploring Protein Conformational Landscapes
761 Using High-Pressure NMR. *Methods Enzymol* **2019,** *614*, 293-320.
762 (51) Zwanzig, R., Two-state models of protein folding kinetics. *Proc Natl Acad Sci U S A*
763 **1997,** *94* (1), 148-150.
764 (52) Kharakoz, D. P., Partial volumes and compressibilities of extended polypeptide chains in
765 aqueous solution: additivity scheme and implication of protein unfolding at normal and high
766 pressure. *Biochemistry* **1997,** *36* (33), 10276-10285.

767 (53) Panick, G.; Vidugiris, G. J.; Malessa, R.; Rapp, G.; Winter, R.; Royer, C. A., Exploring
768 the temperature-pressure phase diagram of staphylococcal nuclease. *Biochemistry* **1999,** *38* (13),
769 4157-4164.
770 (54) Roche, J.; Caro, J. A.; Norberto, D. R.; Barthe, P.; Roumestand, C.; Schlessman, J. L.;
771 Garcia, A. E.; Garcia-Moreno, B. E.; Royer, C. A., Cavities determine the pressure unfolding of
772 proteins. *Proc Natl Acad Sci U S A* **2012,** *109* (18), 6945-6950.
773 (55) Font, J.; Benito, A.; Lange, R.; Ribo, M.; Vilanova, M., The contribution of the residues
774 from the main hydrophobic core of ribonuclease A to its pressure-folding transition state. *Protein*
775 *Sci* **2006,** *15* (5), 1000-1009.
776 (56) Zhang, S.; Zhang, Y.; Stenzoski, N. E.; Zou, J.; Peran, I.; McCallum, S. A.; Raleigh, D.
777 P.; Royer, C. A., Pressure-Temperature Analysis of the Stability of the CTL9 Domain Reveals
778 Hidden Intermediates. *Biophys J* **2019,** *116* (3), 445-453.
779 (57) Zipp, A.; Kauzmann, W., Pressure denaturation of metmyoglobin. *Biochemistry* **1973,** *12*
780 (21), 4217-4228.
781 (58) Royer, C. A., Revisiting volume changes in pressure-induced protein unfolding. *Biochim*
782 *Biophys Acta* **2002,** *1595* (1-2), 201-209.
783 (59) Roche, J.; Royer, C. A.; Roumestand, C., Monitoring protein folding through high
784 pressure NMR spectroscopy. *Prog Nucl Magn Reson Spectrosc* **2017,** *102-103*, 15-31.
785 (60) Taulier, N.; Chalikian, T. V., Compressibility of protein transitions. *Biochim Biophys*
786 *Acta* **2002,** *1595* (1-2), 48-70.
787 (61) Bu, Z.; Callaway, D. J., Proteins move! Protein dynamics and long-range allostery in cell
788 signaling. *Adv Protein Chem Struct Biol* **2011,** *83*, 163-221.

789 (62) Kitahara, R.; Yamada, H.; Akasaka, K., Two folded conformers of ubiquitin revealed by
790 high-pressure NMR. *Biochemistry* **2001,** *40* (45), 13556-13563.
791 (63) Narayanan, S. P.; Nair, D. G.; Schaal, D.; Barbosa de Aguiar, M.; Wenzel, S.; Kremer,
792 W.; Schwarzinger, S.; Kalbitzer, H. R., Structural transitions in full-length human prion protein
793 detected by xenon as probe and spin labeling of the N-terminal domain. *Sci Rep* **2016,** *6*, 28419.
794 (64) Lerch, M. T.; Yang, Z.; Brooks, E. K.; Hubbell, W. L., Mapping protein conformational
795 heterogeneity under pressure with site-directed spin labeling and double electron-electron
796 resonance. *Proc Natl Acad Sci U S A* **2014,** *111* (13), E1201-1210.
797 (65) Roche, J.; Dellarole, M.; Caro, J. A.; Norberto, D. R.; Garcia, A. E.; Garcia-Moreno, B.;
798 Roumestand, C.; Royer, C. A., Effect of internal cavities on folding rates and routes revealed by
799 real-time pressure-jump NMR spectroscopy. *J Am Chem Soc* **2013,** *135* (39), 14610-14618.
800 (66) Kharakoz, D. P., Protein compressibility, dynamics, and pressure. *Biophys J* **2000,** *79*
801 (1), 511-525.
802 (67) Chalikian, T. V.; Breslauer, K. J., Compressibility as a means to detect and characterize
803 globular protein states. *Proc Natl Acad Sci U S A* **1996,** *93* (3), 1012-1014.
804 (68) Beck Erlach, M.; Koehler, J.; Moeser, B.; Horinek, D.; Kremer, W.; Kalbitzer, H. R.,
805 Relationship between nonlinear pressure-induced chemical shift changes and thermodynamic
806 parameters. *J Phys Chem B* **2014,** *118* (21), 5681-5690.
807 (69) Eneqvist, T.; Andersson, K.; Olofsson, A.; Lundgren, E.; Sauer-Eriksson, A. E., The
808 beta-slip: a novel concept in transthyretin amyloidosis. *Mol Cell* **2000,** *6* (5), 1207-1218.
809 (70) Panteva, M. T.; Salari, R.; Bhattacharjee, M.; Chong, L. T., Direct observations of shifts
810 in the beta-sheet register of a protein-peptide complex using explicit solvent simulations.
811 *Biophys J* **2011,** *100* (9), L50-52.